Evolution of the flax cell wall composition during development and after gravitropism by synchrotron fluorescence imaging

Johnny Beaugrand, Camille Goudenhooft, Camille Alvarado, M.F. Devaux, Camille Rivard, Sylvie Durand, Hugo Chauvet, Matthieu Réfrégiers, Frédéric Jamme, Fabienne Guillon, et al.

Evolution of the flax cell wall composition during development and after gravitropism by synchrotron fluorescence imaging

[*a] Johnny Beaugrand, [b] Camille Goudenhooft, [a] Camille Alvarado, [a] Marie-Françoise Devaux, [c,d] Camille Rivard, [a] Sylvie Durand, [e] Hugo Chauvet, [e] Matthieu Réfrégiers, [e] Fréderic Jamme, [a] Fabienne Guillon, [b] Christophe Baley, [b] Alain Bourmaud

[a] INRAE, UR1268 BIA, F-44316, Nantes, France
[b] Univ. Bretagne Sud, UMR CNRS 6027, IRDL, F-56100 Lorient, France
[c] Synchrotron SOLEIL, LUCIA Beamline, F-91192 Gif-sur-Yvette, France
[d] INRAE, UAR 1008 TRANSFORM, F-44316 Nantes, France
[e] Synchrotron SOLEIL, DISCO Beamline, F-91192 Gif-sur-Yvette, France

*Corresponding author: johnny.beaugrand@inrae.fr

Abstract

Flax (*Linum usitatissimum*) lodging is an issue of great interest for industrial producers due to its economic impact; despite a strong varietal selection over around one century, this plant remains sensitive to lodging which represents a main technico-economic issue. To better understand lodging effects at the cell wall and stem scale, the cell wall composition dynamics during cell wall development and after a 90° tilt bending stress is reported. Deep-Ultra Violet fluorescence emission (DUV) dynamics recorded at the Synchrotron SOLEIL-DISCO beamline by multichannel autofluorescence imaging is addressed for five cellular wall types of flax stems after an artificially induced gravitropic reaction. The quantitative fluorescent profile intensities were computed after image

analysis, and compared to the control flax stems, we reported a systematically higher average intensity fluorescence (probability >95%) for the 90° tilted plants. Moreover, the average stem fluorescence intensities were significantly different among the 3 developmental stages, with the youngest stage (VS) exhibiting on average 30% and 20% less fluorescence than the medium (FG) and mature (M) stages, respectively. The flax stem response to tilt impacted the xylem cellular type, while the bast fibres were arguably less affected by the protein, and hydroxycinnamate contents. A complementary investigation was carried out on bast fibres by infrared microspectroscopy to explore the polysaccharide components not seen in deep UV fluorescence, and significant modifications were monitored.

Key words: Flax; Infrared microspectroscopy; Hydroxycinnamate; Proteins; Lignin; Polysaccharide

1. Introduction

One of the oldest fibre plants used by humans is a flax plant (*Linum ~~U~~usitatissimum* L.*)*; traces of flax as far as back the prehistoric civilization in Egypt, ancient Babylonia, and Europe (Heer, 1873) have been verified. Flax, as industrial crop of economic interest, has been used for textile applications, for new developments in the field of high-performance composites in terms of the mechanics (Bourmaud et al., 2018; Mohanty et al., 2018), and for additional functionalities such as acoustic properties, e.g., for violin design (Viala et al., 2018).

Flax belongs to the dicotyledonous group (Ray F. Evert, 2006), and its development has been well documented and recently reviewed (Goudenhooft et al., 2019a). Basically, this temperate crop follows four identifiable growth stages and can be schemed on a cumulative growing degree-day scale, starting from 0°C as the sowing date and reaching

1,000°C at flax stem fibre maturity. From a description point of view, the beginning is the emergence of the plant, followed by the vegetative stage (VS). At 15–20 days of the VS, the flax plant reaches approximately 15-20 cm (approximately 250 growing degree days). Then, for approximately three weeks, FG takes place. At that time, the flax plant elongates up to several centimetres per day (Gorshkova et al., 1996; Heller et al., 2015), reaching 80–90 cm over this fast FG period (approximately 500 growing degree days). The flax stem reaches a final length of approximately 1 m (Gorshkova et al., 2003) at fibre maturity (M) (approximately 1000 growing degree days).

Some external stresses may impact the bast fibre yield and benefits, such as the lodging phenomenon (Goudenhooft et al., 2019b), a stress of economic importance due to its high impact on farmer incomes. From a fundamental view, it is fascinating to note that flax stems can be restored from lodging through a gravitropism reaction under specific conditions, such as the plant response to gravity after tilting (Ibragimova et al., 2017). Goudenhooft et al. (Goudenhooft et al., 2019b) reported a decrease into mechanical properties of single fibres between the not-tilted flax fibres and tilted flax fibres, especially for young plants, with almost no difference between the not-tilted /tilted flax fibres at plant maturity. Among the stem cell types, bast fibres are actors in the plant gravitropic reaction through the adjustability of their cell wall performance (Goudenhooft et al., 2019b), but the implication of other cellular types, such as xylem, has also been demonstrated, with a significant evolution of the xylem cell morphology and structure after the tilt stage (Petrova et al., 2021). At the scale of the flax stem, the focus has often been on the bast fibres, which is the reinforcement element of the flax stem (Goudenhooft et al., 2018; Réquilé et al., 2018). In addition, substantial work have been done on the bast fibre from the pulling side of the flax stems tilted at the VS, those cells even displayed an increased cell diameter and an enlarged lumen (Ibragimova et al., 2017).

77 Flax polysaccharides arguably represent the main component of the stem in terms of the
78 mass, with cellulose being the major component in both xylem (Beaugrand et al., 2014;
79 Nuez et al., 2020) and bast fibres (Bourmaud et al., 2019). For instance, the stem
80 epidermis covered by a cuticle, the cambial layer and the primary and secondary xylems
81 have been less documented (Lion et al., 2017).
82 In the flax stem, some biochemical compounds are naturally fluorescent, including
83 aromatic substances or compounds containing conjugated double bonds, and this
84 property can be used for detection via fluorescence imaging techniques. For example,
85 lignins and hydroxycinnamate exhibit intense fluorescence in the UV and visible regions.
86 In proteins, the dominant fluorophore is the indole group of tryptophan, which absorbs
87 near 280 nm and emits approximately 340 nm. In particular, synchrotron radiation
88 provides deep-UV illumination (DUV), enabling multipurpose molecular fluorescence
89 identification (Giuliani et al., 2009). Using a synchrotron source, a spatial resolution
90 compatible with the sizes of the cell and cell wall (10–50 µm and 1–5 µm, respectively)
91 can be attained with a good signal-to-noise ratio (Allouche et al., 2012). The excitation at
92 275 nm coupled with an emission in the range 327-353 nm makes it possible to visualize
93 the proteins thanks to the natural fluorescence of tryptophan and tyrosine, which they
94 harbour in their amino acid sequence (Jamme et al., 2014). Using the same excitation
95 wavelength, phenolic compounds exhibit natural fluorescence and can be detected at the
96 cell wall scale in lignocellulosic plants at an emission over 380 nm (Devaux et al., 2018a).
97 Because of fluorescence emission bandpass filters, hydroxycinnamate acids can be
98 partially distinguished from lignin-polymerized phenolic components. Indeed,
99 fluorescence emission bandpass filters at 420-460 nm and 480-550 nm can be used to
100 highlight hydroxycinnamate acids and lignin differentially (Jamme et al., 2013).
101 Since polysaccharides are not autofluorescent, mid-infrared (FTIR) spectroscopy has
102 been used to track polysaccharide compositions. Indeed, FTIR microspectroscopy has

proven its value in monitoring hemicellulose metabolism in flax (Chabi et al., 2017). Additional work has highlighted the interest of this approach for flax, examining growth-induced modifications of cells (Stewart et al., 1995). In this study, Stewart et al. reported the spectra of bast fibre cell walls with a predominance of cellulose absorbance. In addition, this work suggested the presence of acetylated hemicelluloses (xylan and/or glucomannan).

In addition to the polysaccharidic components, protein and phenolic compounds play also a major role on metabolism and defence mechanisms of flax cell walls. Major achievements have been reported regarding flax protein expression (Corbin et al., 2013), as well as genome identification and evolution patterns of the main protein family according to differential regulation (Corbin et al., 2018). In addition, phenolic compounds such as hydroxycinnamates are most often esters linked to polysaccharides and esters or ethers linked to lignin monolignols. These compounds can act as interpolymer coupling agents, for example, between polysaccharides and lignin or polysaccharides and structural proteins containing tyrosine amino acids. Hydroxycinnamates, such as lignans, also play an important role in plant defence (Mnich et al., 2020). An attempt to identify and localize phenolic compounds in cell walls by microscopy was made using a laccase tagged with colloidal gold; this enzyme was able to bind to phenolic compounds (Gorshkova et al., 2000). The authors revealed several gold particle distribution patterns, with compact labelling in xylem and bast fibres; a large proportion of bast fibre wall phenolics consisted of phenolic acids rather than lignin. Lignin is often described as a 3D phenolic polymer (Liao et al., 2020). In flax, lignin is mainly concentrated in xylem, and the bast fibre lignin content is very low. The spatial regulation of constitutive lignin under development or during stress is ~~well~~ documented (Le Roy et al., 2017). The xylem histological part of the stem was particularly well investigated with an elaborate chemistry strategy coupled with a creative microscopic investigation (Lion et al., 2017).

129 The general basics regarding flax plants, their developmental stages and bast fibre
130 characteristics is address in the literature with some recommended papers (Goudenhooft
131 et al., 2019a; Petrova et al., 2019), but the study of the impact of stress on the cell wall
132 biochemistry or ultrastructure of other flax stem cell types is sparse.
133 In the current study, FTIR microspectroscopy was performed on only bast fibres. This
134 choice is motivated by the economic interest of that fibre and because it is well
135 documented in the literature in comparison to the others type of cell.
136 The purpose of this research is to monitor when, where and with what amplitude the
137 biochemical components in flax varied using FTIR (bast fibre only) and deep UV
138 fluorescence after a gravitropic event. Two conditions were chosen: i) during the normal
139 growth of the flax plant as a control plant and ii) following severe stress, namely, 90°
140 bending, which generates gravitropism. These two growing conditions were combined
141 with the three main stages of flax development (vegetative, fast growth and mature
142 stage), and for each, the proteins, hydroxycinnamate and lignin distributions and relative
143 amounts were studied for the five stem cell types investigated.
144

145 **2. Material and methods**

146 2.1 Flax stems, sampling protocol and growing conditions

147 Flax plants (*Linum usitatissimum* L., Bolchoï, seeds provided by Terre de Lin, France)
148 were studied. This variety is ~~this variety~~ is dedicated to the production of ~~fiber~~ fibre. The
149 protocol followed is described in (Goudenhooft et al., 2019b). Briefly, seeds were sown in
150 pots and cultivated outdoors (Lorient, France) in 2017 at a conventional seeding rate of
151 approximately 1800 seeds/m² (Bourmaud et al., 2016).
152 A control (C) batch containing plants that never tilted was used as a reference. Three
153 additional pots were used for the experiments, consisting of pots inclined at
154 approximately 90° at different key stages of plant development (Fig 1).

Figure 1

The first pot was tilted at the beginning of the VS, when plants reached approximately 25 cm, 29 days after sowing and a cumulative temperature of 370°C. The second pot was inclined during the FG period, when plants were approximately 50 cm, 40 days after sowing and 510°C of cumulated temperature. Finally, the third pot was tilted at plant maturity (M), in the present case when plants were approximately 80 cm, 77 days after sowing and when the cumulative temperature reached the expected 1000°C (Goudenhooft et al., 2017).

At each stage of tilting, some plants were sampled. Immediately after sampling, stem portions were fixed overnight in a solution of 4% v/v formaldehyde in 0.1 M phosphate buffer (pH 7.2) at 4°C.

2.2 Deep UV Fluorescence imaging at the SOLEIL synchrotron DISCO beamline

The DISCO beamline and the imaging microscope setup have been fully described in Giuliani et al.(Giuliani et al., 2009) and in Jamme et al. (Jamme et al., 2013). The so-called TELEMOS microscope is a modified full-field microscope (Axio Observer Z1, Carl Zeiss GmbH, Germany) coupled to the monochromatized synchrotron beam. The power delivered on the sample at the DISCO beamline imaging branch is limited to a few microwatts (1.1*10-6 W at 280 nm). This value avoids beam photodamage by deep UV absorption. The synchrotron beam aligned and focused on the sample using an Ultrafluar 40x (NA 0.6) objective provides a field of view of 250*250 μm^2 with a pixel size of 244 nm. The microscope is equipped with a 16-bit back-illuminated CCD camera (Pixis BUV, Princeton Instrument, USA) that allows 65536 grey levels to code the fluorescence intensity and an image size of 1024 x 1024 pixels. The acquisition of images is driven by the ImageJ plugin µManager (Edelstein et al., 2010).

180 The excitation wavelength was set at 275 nm. A dichroic mirror at 300 nm and three
181 bandpass filters were used for the acquisition of multispectral images. The emission filter
182 at 327-353 nm selected the fluorescence of tryptophan and tyrosine found in the proteins,
183 and the emission filter at 420-460 nm made it possible to acquire images of phenolic
184 compounds corresponding to both the hydroxycinnamic acids and lignin. The emission
185 filter at 480-550 nm was retained as a more specific lignin (Frédéric et al., 2013) however
186 more recent investigations has shown that other phenolics compounds like flavonol,
187 condensates tannins, anthocyanins can fluorescence in the same range as lignin do
188 (Vidot et al. 2019). Therefore, the signal collected between 480-550 nm cannot guarantee
189 the solely ~~the~~ lignin emission. Image acquisition was performed at room temperature,
190 and the acquisition time was set to 10 s for the three filters. Finally, visible images in
191 transmission mode were acquired in the sequence of multispectral acquisition. The
192 acquisition time was set to 100 ms for the transmission images.
193 The reference images for background and illumination heterogeneities were acquired
194 once per day, and the run of the entire acquisition covered 3 days. The background
195 images corresponded to the signal recorded by the camera without any illumination and
196 any sample. Using the current camera, the background level was approximately 700 and
197 depended on the filter, acquisition time and location in the image. One background image
198 per bandpass filter was acquired by setting the acquisition time accordingly to 10 s. The
199 illumination field depends on the synchrotron beam alignment and the focal plane. The
200 images of the illumination were acquired using a luminescent reference compound (Nd-
201 YAG crystal) using only the dichroic mirror without any filter and setting the acquisition
202 time to 250 ms. A Z-stack of 101 images was acquired with a 2 µm step between each
203 image.
204 Flax stem whole sections with a 45 µm thickness were obtained using a HM650V
205 vibratome (Microm International GmbH, Waldorf, Germany) and were deposited on a 1”

206 diameter quartz coverslip (R525000, Esco Optics). Just before the acquisition, the
207 sections were mounted in distilled water and sandwiched with a second circular quartz
208 coverslip. A 10× (NA 0.2) Ultrafluar Zeiss (Carl Zeiss GmbH, Germany) lens was used to
209 provide a field of view of 1.116 × 1.116 µm² with a pixel size of 1.092 µm. Stem sections
210 were approximately 3-4 mm large, and a single image was not sufficient to observe the
211 whole section. A series of images were acquired to cover the whole surface of the section
212 after defining a region of interest in the centre of the images that corresponded to the
213 region illuminated by the synchrotron beam. Depending on the section, between 20 and
214 30 individual images were acquired to scan the whole section.
215
216 2.3 Fluorescence image preprocessing and analysis
217 The fluorescence intensity around the stem section was examined for the 5 cell types
218 including the epidermis (ep), the bast fibre (bf), the cambium (ca), the primary (px) or the
219 secondary (sx) xylem shown in Fig 2f.
220 Figure 2
221 The specific cell type intensity measurements were obtained by manual selection of the
222 pixels (Fig 4B). The fluorescence intensity of the cell types was measured for the three
223 filters as the average intensity of the selected pixels. This measurement was repeated for
224 each of the 4 quarters of the stem.
225 The fluorescence intensities were averaged over the 2 repetitions of measures in the four
226 quarters of the stem (= 8 measures of fluorescence intensity itself corresponding to the
227 average value along the selected pixels as shown in figure 4 and explained in paragraph
228 2.3 Fluorescence image preprocessing and analysis). The average values shown in figure
229 5 and 6 are computed during the variance analysis and show the effect of the two factors
230 development and tilting conditions.

Fluorescence images were preprocessed in Devaux et al. (Devaux et al., 2018b) using the principles described in Tomazevic work (Tomazevic et al., 2002) for shading correction. The goal was to remove the camera background and compensate for the illumination inhomogeneity using eq 1:

$$\mathrm{IMC}(\lambda) = \frac{(\mathrm{IM}(\lambda) - \mathrm{BKG}(\lambda))}{\mathrm{ILL}(z)} \qquad \text{eq (1)}$$

where IM(λ) is the raw image acquired using filter λ, BKG(λ) is the additive background, ILL(*z*) is the z^{th} image of the illumination reference Z-stack and IMC(λ) is the preprocessed image. In the present work, the z^{th} illumination image was obtained by 1) calculating an illumination image as the maximum intensity of all individual images of the section and 2) selecting the z^{th} image ILL(*z*) in the illumination reference Z-stack as the most correlated to the estimated illumination image. The main steps of image preprocessing are illustrated in the Supplementary Data section.

Supplementary Data section

Images of the whole section were finally built for the three emission filters by merging the preprocessed images into three mosaic images, called composite images, using the information provided by the moving stage. The intensities at the stitching interfaces were set to the maxima between the two adjacent individual images.

Fluorescence image analysis included image observation and fluorescence intensity measurement for each given cell type.

Table 1

False colour images were built from the three emission filters, as described in Table 1. In the resulting colour images, the regions rich in proteins are identified as mainly blue regions, the regions rich in hydroxycinnamates are identified as green regions, and the regions rich in the assumed lignin signal are identified with a colour varying between yellow and red (see Fig 2).

256 Fluorescence intensities were measured in the images for each filter by manually
257 selecting pixels corresponding to different cell types: epidermis (ep), bast fibres (bf);
258 cambium (ca), secondary xylem (xs) and primary xylem (xp). For each cell type, two sets
259 of pixels were selected from each of the four quarters of the section. The intensities were
260 averaged over pixels, resulting in 5 cell types x 4 quarters x 2 repetitions x 3 filter
261 measures per image. The intensities were compared using variance analysis by
262 considering three experimental factors: development stage, tilting conditions, cell types
263 and their interactions.
264 Image processing and variance analyses were performed using MATLAB 2019a with the
265 commercial 'Statistics and Machine Learning' toolbox' (The MathWorks, France).
266 Fluorescence profiles were extracted using a home made Matlab software allowing the
267 multispectral analysis of the images. Variance analysis was performed using Matlab
268 anova function. The methods allow to recover the mean values and the standard
269 deviations of the effect tested.
270
271 2.4 Fourier transform infrared microspectroscopy - spectral analysis
272 Small cylinders (approximately 5 mm in length) of flax stems from the 3 development
273 stages (see section 2.1 and Fig 1), under normal conditions and under stress with a 90°
274 tilt, were embedded in paraffin (Automate Tissue Tek VIP 3000). Sixteen thick cross
275 sections were obtained using an HM355S microtome from Microm and were collected on
276 ZnS windows. The sections were submitted to a Histochoice clearing agent (Sigma
277 H2779) solution to remove the paraffin.
278 Localized spectra were acquired by mid-infrared microspectroscopy using a Tensor 27
279 (Bruker Optics) spectrometer equipped with a Hyperion 2000 microscope (Bruker Optics).
280 Visible images were obtained using a Sony camera (Exwave HAD, SSC-DC80P). A 36x
281 objective was selected, and depending on the cell sizes and stage of development, an

aperture of 400 to 1600 µm² was set. Infrared spectra were collected in the 4000-700 cm^{-1} range at a resolution of 8 cm^{-1}. Each spectrum summed 700 scans for the background and 500 scans for the samples.

All spectra were baseline corrected and normalized using the acquisition software OPUS7.5 (Bruker optics). The spectra were cropped to the 2000-700 cm^{-1} range, highlighting the polysaccharide region of interest for the bast fibre components. Norris gap second-derivative spectra were assessed using Unscrambler software (version 10.1, Camo). The second-derivative spectra were thereafter multiplied by (–1).

3. Results and discussion

3.1. Qualitative analysis of the fluorescence images according to development stages and tilting conditions

Fig 2 shows the fluorescence images of the flax stem cross sections at the young development stage for the control plant for the three filters 327-353 nm (Fig 2a), 420-460 nm (Fig 2b) and 480-550 nm (Fig 2c) corresponding to proteins, hydroxycinnamate and lignin, respectively, and the composite view (Fig 2d). One can visually observe that the intensities are different between channels and that the fluorescence signal seems uniform all around the section circumference. The protein fluorescence is mainly located in the secondary xylem. The hydroxycinnamate fluorescence is intense in the cambial tissue and more diffuse in the xylem areas (Fig 2b). However, due to the size resolution of the beam and the very small size of the cells and walls, the signals recovered in the cambium (ca) is likely to mix the fluorescence of the cytosol and the wall. The lignin fluorescence is stronger in the xylem area. The epidermis fluorescence is the most intense in the hydroxycinnamate (Fig 2b) and lignin (Fig 2c) channels, whereas only a slight signal is visible in the protein (Fig 2a) channels. Although we selected carefully bandpass filters to collect the fluorescence emission of the hydroxycinnamate and lignins separately, we

cannot exclude a partial overlap of the emission spectra of these compounds, and caution should be taken when assigning the signals in absolute values. Finally, one can notice that in the inner part of the stem, the parenchymatic cells do not fluoresce much regardless of the channel used. The three images were combined to obtain a composite colour image that reveals the distribution of the three fluorescence signals (Fig 2d, composite). The proteins are identified in the blue channel, while the hydroxycinnamates are given by the green channel, and the lignin is depicted by the red channel (Fig 2e). ~~The interpretation of the colours obtained is sometimes tricky and requires the quantification of the individual fluorescence intensity, which will be presented below~~. A quarter of the stem section was stained with phloroglucinol and zoomed in the picture f (Fig 2f). One can follow from the outer part of the stem to the inward epidermis (ep). Then, the thick bast fibre wall is arranged in bundles (bf), followed by an area of several layers of small and active cells where the cambial area is located. The cambial cells are small and full of cytoplasm, it is expected that the fluorescence intensity signal recorded there will mix the fluorescence of the cytosol and the wall. Further on, we can see the xylem stained in red due to its high content of lignin, the xylem divided into (xs) as the youngest secondary xylem, and finally the oldest xylem as (xp) is the primary xylem build-up by the plant.

Figure 3

Fig 3 shows the composite fluorescence images of the flax stem cross sections using the same spatial scale for different maturity stages and the control versus 90° tilted conditions obtained following the procedure illustrated in Fig 2.

<u>Evolution according to the development stage</u>

The first qualitative information is that during the development of the control plant (Fig 3 a-c), a global intensity decrease is observed. The mature stage M_C (Fig 3 c) displays a lower fluorescence intensity, and the protein signal is almost extinct at this oldest stage.

These observations also apply to bast fibres, with some traces of hydroxycinnamate and proteins at the MS. For FG and M stages, the protein signal is intense in the cambial area (Fig 3b) ~~and in~~ an active epithelium if any. The fluorescence intensity of the xylem area increases as the stem matures with a shift from blue green to green-yellow fluorescence. ~~This shift is attributed to a decrease in proteins involved in cell wall metabolism as the stem ages (Fig 3c).~~ The outer xylem part, located close to the cambium, always shows more intense fluorescence. The inner region of xylem shows green-yellow fluorescence, corresponding to the hydroxycinnamates and lignin channels, regardless of the considered developmental stage. Previous work has shown that during the starting stage of lignification, the structure of lignins can evolve; for herbaceous plants such as flax, lignin mainly originates from the polymerization of trans-para-coumaryl alcohol (Day, 2004). Lignins can also be linked to cell wall proteins (Monties, 1989) and to phenolics, ferulic or *p*-coumaric acids (Scalbert et al., 1985) (Monties, 1989). Thus, during the implementation of lignin, its structure can take different configurations related to the different fluorescence responses.

Evolution related to the tilted effect

~~For the 90° tilted plant, the evolution is not as linear as that during the development stage~~ For the plant inclined at 90 °, the evolution is more contrasted than during the development phase of the control plants. VS_90 presented more green fluorescence than FG_90 and M_90. More blue fluorescence is seen in FG_90 than in the two other stages. When the gravitropic response takes place during the VS, the cambial region is more intense than the control (see Fig 3a&d), suggesting greater cambial ~~activity~~metabolism with tilting. In the VS, the main difference is a more intense green ring visible in the innermost stem tissue, corresponding to the primary xylem. One hypothesis to explain this modification could be a consequence of a modification of the transport in the plant, probably of the sap after the curving of the stem, which could induce a mobilization or

translocation of hydroxycinnamates. ~~It is generally admitted that primary metabolic activity is reflected by the presence of proteins (Buchanan et al., 2000). These proteins are cell effectors, structural proteins, etc. involved in the major processes of living organisms and cells. Arguably, hydroxycinnamate is a secondary metabolite. Their localization and modifications therefore reflect metabolic activity but are not as strong as the primary metabolism of proteins.~~

The restoration of the plant vertical position also occurred in the FG period (Fig 3 b&e). During this step, the cambial region of tilted samples (Fig 3e) also seemed to be more fluorescent than the control samples (Fig 3. d). The protein signal areas and intensities (blue) were more pronounced, with the bast fibres being greener fluorescent (hydroxycinnamate) than the control plants.

During the gravitropic reaction (Fig 3 c&f), a much higher fluorescence intensity was observed at M_90 than at the control M_C. Despite the presence of well-mature cell walls, ~~especially in the primary tissues,~~ the cambial ~~activity~~ fluorescence of tilted plants (Fig 3f) was still present but more limited than that of tilted plants at the younger stages, as shown by the reduction in the blue xylem “ring” in contact with the cambium (Fig 3 d&e). Moreover, the area and intensities of the signals coming from hydroxycinnamates are much greater than those from any other samples, proving that mature cells are still able to react to ~~inclination~~bending. ~~This reaction most likely affects the lignification process or lignin cellular types such as xylem and hydroxycinnamate, which are precursors of this cell wall component.~~

It seems by eye that mature fibres are not strongly involved in the gravitropic reaction, whereas the xylem secondary part is. In addition, regarding the bast fibre, the signal intensities of M_90 seemed lower than those of tilted plants from previous growth stages and were similar to those of the control M_C plants.

385 Finally, no polarisation of the signal in response to tilting is analysed ‘by eye’ observation.
386 This comment is mandatory because a polar gravitropic response is possible, visible at
387 the scale of the stem between the opposite and bending sides (Ibragimova et al., 2017).
388 Indeed, it has been reported that some morphological modifications in response to
389 gravitropism can take place in the bast fibre but only when bending takes place at a
390 juvenile plant stage.
391 This qualitative observation of the signals by eye offers information, but quantitative
392 information would provide more information. Therefore, we measured the fluorescence
393 intensity on the cross sections, as explained ~~later~~ below.
394
395 3.2. Fluorescence quantitative analysis according to the development stages and tilting
396 conditions
397 For a quantitative fluorescence analysis, an arbitrary virtual division of the stem section
398 into four quarters, called 1 to 4, was performed, as illustrated in Fig 4 A.
399 Figure 4
400 The fluorescence intensity collected for each filter allows quantitative evaluations in the
401 fluorescence count unit.
402 From those average fluorescence intensity values, an analysis of variance (ANOVA) was
403 performed for each filter (Fig 5).
404 Figure 5
405 The developmental stage, tilting, cell types and all interactions were found to be
406 significant. Because proteins, hydroxycinnamates and lignin arguably do not fluoresce in
407 the same manner and in the same environment, a higher fluorescence does not
408 necessarily mean higher molar amounts; therefore, it is not possible to compare the
409 different components as molar amounts based on their respective signals. If we focus first
410 on the development stage effect, then the average fluorescence intensity for the three

411 emission channels ~~corresponding to proteins (Fig 5a), hydroxycinnamates (Fig 5b) and~~
412 ~~lignin (Fig 5c)~~ varied between the 3 development stages. The highest intensity for
413 proteins and hydroxycinnamates was observed in the fast growing stage for both the
414 control and 90° tilted stems (FS_C or FS_90), and the lowest intensity was observed in
415 the vegetative stage (VS_C or VS_90°). This trend is different for lignin: an increase in
416 the intensity occurred between stages VS and FG before reaching a plateau. In contrast,
417 the lignin fluorescence seemed equal for the three developmental stages of the 90° tilted
418 stems. If we focus now on the tilt effect, then the gravitropic response systematically
419 induced an increase in the fluorescence intensity in the three channels compared to the
420 control plant stems, by 51, 28 and 23% for proteins, hydroxycinnamate and lignin,
421 respectively. The 90° tilt gives rise to an average increase of 32% of the fluorescence
422 (Fig 5), somehow confirming the qualitative observation (section 3.1, Fig 2). This result
423 suggests a global boost in plant metabolism following lodging stress.
424
425 *3.2.1 At the cell type scale, evolution according to development stage*
426 To go further in the analysis, we looked at the fluorescence intensity according to the cell
427 types.
428 Figure 6
429 ~~Fig 6 presents the average fluorescence intensity for the 5 cell types related to their~~
430 ~~developmental stage and tilt condition.~~ The epidermal protein intensity signal was weak
431 and did not change according to the VS and the FG and M stages of the control plants
432 (Fig 6). The hydroxycinnamate fluorescence signal is more intense and remains stable.
433 The highest fluorescence intensity was measured for lignin, but the standard deviation of
434 the average values was so large that no significant trend could be deduced. Here, the
435 very thin layer of the epidermis is arguably a technical limitation with respect to the pixel

436 resolution, which might explain in part the importance of the standard deviation (SD)
437 observed.
438 Bast fibres are thicker, and the SDs are very small regardless of the constituent under
439 consideration (Fig 6, second line of histogram). The intensity of protein fluorescence
440 increased between the VS and FG stage and then decreased between the FG and M
441 stages in the control plants. The intensity of the hydroxycinnamate fluorescence
442 remained almost unchanged between the VS and FG stage and then decreased at the M
443 stage. The lignin signal evolves accordingly, with only a decrease at stage M. Scarce
444 literature deals with the quantification or localization of lignin in bast fibres, and a recent
445 report based on safranin ratiometric image investigations on flax stem cross sections has
446 presented a slight increase in the lignin content of mutant plants during cell development
447 (Baldacci-Cresp et al., 2020).
448 Due to the economic importance of flax bast fibres, more literature is available regarding
449 their composition (Akin, 2013; Bourmaud et al., 2018; Bourmaud et al., 2019) and
450 evolution during plant growth and in response to stress (Goudenhooft et al., 2019a). In
451 connection with Fig 3, the colour of the bast fibre evolves with maturity; in the FG stage,
452 the blue colour representing mainly proteins is evident with a homogenous colour within
453 the fibre cell wall, indicating probably the achievement of the transformation of the
454 immature Gn wall into the mature G at this stage (Gorshkova et al., 2003). This
455 qualitative observation is supported by the protein fluorescence peak observed in Fig 6
456 (see FG-C, ‘Bast Fibre Proteins’). The structure of bast fibres has been demonstrated to
457 be progressive, with a first Gn layer composed of cellulose and long galactan chains
458 evolving towards a more structured G layer. In this new and mature layer, the length of
459 galactan chains is reduced under the action of galactosidase enzymes, inducing their
460 entrapment between cellulose microfibrils (Gorshkova et al., 2015) and a more cohesive
461 and stiff (Arnould et al., 2017) structure. Here, protein family identification is not possible

since we indifferently detected all tryptophan that belongs to the whole protein class. However, an increase in AGP and extensin during flax fibre development is more likely (Day et al., 2013).

The cambium fluorescence signals (third line of histogram, Fig 6) for proteins, hydroxycinnamates and lignin show similar trends to the bast fibre, i.e., an increase between the VS and FG stage, followed by a slight decrease in the M stage. The fluorescence intensity in cambium is rather high, and the variations between developmental stages are marked.

The secondary xylem (xs) cells demark with the other cell wall types. Indeed, for fluorescence signals attributed to hydroxycinnamates or lignin, there was a significant decrease from the VS to the M stage. The protein fluorescence is higher than that of the other cell types, and signals for proteins fall drastically between the FG and M stages. In contrast, for the signals attributed to hydroxycinnamates and lignins, the decrease is progressive between the VG and M stages. Regarding lignin, a recent report using an elegant tag of lignin specifies the active areas of lignification in the secondary xylem of flax (Lion et al., 2017). The authors showed temporal lignification differences among the xylem vessel, ray parenchyma cells and tracheid cells, as well as revealing the polarization at the scale of a single-cell lignification dynamics. In this work, such resolutions could not be achieved, but we observed a slight decline in the fluorescence intensity in stages FG and M compared to the VS (Fig 6).

Finally, the cell walls of the xylem primary seem to display a unique dynamic over developmental stages, as no significant variations could be detected from the VS to the M stage, regardless of the three biochemical components targeted (Fig 6).

3.2.2 At the scale of the cellular type, evolution according to the 90° tilt stress

The epidermis (ep) fluorescence signals of the proteins, hydroxycinnamates and lignin did not seem to change in stems after 90° tilt stress (Fig 6). The gravitropic response may also be difficult to detect in this thin layer due to an important SD that could mask a moderate physiological plant response.

For the cambial area, all 3 biochemical families exhibited a stronger intensity after tilt, regardless of the maturity stage considered. This finding highlighted the impact of gravitropism on the cambial response and the preponderant function of this tissue in the plant reaction.

The xylem secondary cell wall type is affected by the gravitropic response that follows the 90° tilt (Fig 6). Regarding the protein, signal intensities ~~Indeed, the intensities~~ in FG and M stages were significantly higher than those in the controls. The hydroxycinnamate signals were more intense in the VS and the FG and M stages than in the control stems. The lignin signal follows the same trend but with a smaller contrast between controlled and tilted plants.

The xylem primary cell wall type revealed only an increase in the protein signal at the FG stage. In contrast, for hydroxycinnamate, the FG stage is the only stage unaffected by the 90° tilt stress. Compared to control stems, the lignin signal was higher in both the VS and the M stage, but the FG stage was unaltered.

Finally, the bast fibre after 90° tilt could be expected to be involved in the response of the plant. Tilting is known to disrupt normal fibre thickening and lignification in tension wood fibre walls (Ghislain and Clair, 2017). Here, the fluorescence intensity recorded for proteins does not support a modification of the protein within the cell wall if tilt occurs in the VS or FG stage. ~~The protein signals were unchanged between the control and tilted plants,~~ in accordance with both our visual observations (Fig 3) and with the findings of Goudenhooft et al. (Goudenhooft et al., 2018). However, a slight protein signal increase

was observed if tilt occurred in the M stage. Tilting induces an increase in the hydroxycinnamate signal, and the highest difference between tilting and control plants was observed during the FG stage. For lignin, all tilted plants harbour a slight increase in the fluorescence compared to the control plant, and lignin is a well-known polymer involved in plant stress mechanisms.

3.3 FTIR on the bast fibre

To supplement the deep UV fluorescence examination of the 5 cell types, a study was performed by FTIR microspectroscopy to investigate the polysaccharide composition; ~~this method has been successfully performed on wood fibres (Gierlinger et al., 2008) and flax mutant plants (Dymińska et al., 2014).~~ We focused on the most targeted cell type of the flax stems in the literature, namely, the bast fibres.

FTIR and the development effect on bast fibre

Figure 7

A micro-FTIR investigation was performed on the bast fibre cellular type.

Fig 7A illustrates the location of micro-FTIR spectra in a flax stem section. An average spectrum was calculated, and the assignment of the main absorption bands to biochemical compounds is presented in Fig 7B. The main mass at 1200-700 cm^{-1} is assigned to polysaccharides, such as cellulose, and heteropolysaccharides, such as hemicelluloses and pectin.

The band at approximately 1460 cm^{-1} is assigned to the CH_2 bending of lipids when associated with the C-H_2 stretching bands at approximately 2850 and 2920 cm^{-1} (not shown). The bands at 1735 and 1245 cm^{-1} correspond to esters, while the absorption bands at approximately 1640 and 1540 cm^{-1} are signatures of the presence of proteins. The 1640 cm^{-1} band also refers to fibre internal water.

Figure 8

537 The second-derivative spectra were processed to increase spectral differences in the
538 1800-700 cm^{-1} region (Fig 8). Cellulose, the major constituent of flax fibres, is identified by
539 the spectral bands at 898, 995, 1010, 1030, 1060, 1105 and 1160 cm^{-1} (Maréchal and
540 Chanzy, 2000). The hemicelluloses, O-acetylated glucomannan, xylan and xyloglucan
541 are also present in flax fibre absorbed in the same spectral region as cellulose but can be
542 revealed by the shoulder at approximately 940 and 815 cm^{-1} (Himmelsbach et al., 1998).
543 The youngest development stage (Fig 8) differs from the later stages by bands assigned
544 to lipids (1735 and 1460 cm^{-1}) and adsorbed water (1640 cm^{-1}). The peak at 1010 cm^{-1} is
545 associated with two shoulders at approximately 1600 and 1430 cm^{-1}, assigned to
546 carboxylate symmetric and antisymmetric COO^- bands, which correspond to residual
547 pectin. Its methylated or acetylated form is also present by bands at 1735 and 1245 cm^{-1}.
548 The variation in band intensities assigned to cellulose and hemicelluloses at 1010 and
549 1050 cm^{-1} mainly arises from the change in the pectins/cellulose or cellulose
550 conformation ratio. ~~Regarding the non-cellulosic polysaccharides,~~ pectic galactan, as well
551 as their processing enzymatic machinery (Goubet and Morvan, 1993), are known to be
552 part of the bast fibre and evolve according to cell wall modelling (Mikshina et al., 2012),
553 while galactan and ~~and~~ proteins capable of modifying it play a role with cellulose within
554 Gn to G development (Gorshkova et al., 2004; Roach et al., 2011).
555 FTIR and tilt effect on the bast fibre
556 Figure 9
557 When comparing FTIR signals from the control bast fibre and after tilting (Fig 9), the
558 spectra of the youngest VS bast fibre from 90° tilted plants presented absorption bands
559 from 1105-1050 cm^{-1} with a higher intensity (Fig 9A). This result suggests an increase in
560 the cellulose and hemicellulose contents for the bast fibre of tilted plants. Comparable
561 trends have already been reported with some genetically modified flax lines, with
562 modification of the cellulose ultrastructure and allomorphs in particular (Dymińska et al.,

563 2014). For the FG stage, only slight differences were observed between the control and
564 the 90° tilted plant fibres, ~~corresponding to variations~~ in the absorbance intensity bands
565 assigned to cellulose and hemicelluloses (995, 1030, 1050 and 1060 cm^{-1}) (Fig 9B). At
566 the MS, most of the signals of the 90° tilted FG spectra are close to those obtained for
567 control plants (Fig 9C), but the two bands drastically differ at 1105 and 1050 cm^{-1},
568 indicating that there is also a change in cellulose and a broader panel of polysaccharides
569 between these two conditions.
570
571 3.4 Seeking a stem polar effect on bast fibres by quantitative analysis of the fluorescence
572 To confirm the qualitative conclusion of the absence of polarity between the stem sides
573 (Fig 3), we quantified the fluorescence according to the localization of the pixel selection
574 in the whole circumference of the stem, with a more continuous position resolution (Fig
575 10). For that purpose, in the stem sections of control (M_C) and tilted plants (M_90), we
576 measured the fluorescence from an initial '0' point arbitrarily located.
577 Figure 10
578 Then, we performed a full walk on bast fibres where pixels were selected at different
579 positions all around the stem circumference (Fig 10 a), with at least one set of
580 measurements every 30°. No significant variations in any of the three channel
581 fluorescence intensities can be observed, as seen in the average value linearized
582 according to the angle of measurement (Fig 10 c). Indeed, although an up and down
583 trend can be observed for each of the fluorescence channels, there is no trend for a
584 higher or upper side of the stem with more proteins, hydroxycinnamates or lignins. The
585 tilted stem section showed the highest fluorescence intensity, confirming the
586 quantification of the bast fibre in Fig 6 and the ANOVA (Fig 5). Under our experimental
587 conditions, the 10 cm stem samples collected (starting from 2 cm above the cotyledons),
588 ~~which~~ correspond to the lasting curvature zone when recovery takes place. A comparison

589 with side effects reported in the bast fibre shows an induced morphological change on the
590 bast fibre on the pulling stem side compared to the opposite stem side and control plants,
591 and only if the tilt was at the stage of the G-layer deposition (middle and lower part of
592 stem) (Ibragimova et al., 2017). We hypothesize that this effect is not observed in our
593 report because we may not have sampled the same stem section; for instance, 10 cm
594 long samples were taken 2 cm after the cotyledon versus sampling 1 cm after the
595 cotyledon (Ibragimova et al., 2017). ~~In other words, we may have bypassed the area~~
596 ~~where this polarity occurred, probably by sampling slightly too far in the stem, even if the~~
597 ~~stem sampling area was slightly curved.~~
598
599 **4. Conclusion**
600 The aim of this work was to gain new insights into the dynamics of the cell wall
601 composition in the different cell types of the flax stem during plant development and after
602 a 90° tilt bending stress. The autofluorescence properties of proteins and phenolic
603 compounds when excited at a deep UV (DUV) wavelength accessible to the SOLEIL
604 synchrotron and multichannel fluorescence imaging have made ~~it~~ possible to track
605 proteins and hydroxycinnamates. At contrary, ~~whereas~~ the quantification of the lignin
606 fluorescence by the 480-550 nm filter could not be attained is our case. The specificity of
607 this filter was checked on extracted polymers. In our work, the higher amount of
608 fluorescence observed using this filter in both epidermis or cambium compared to xylem
609 cannot be assigned to lignin. We hypothesis that non-polymeric molecules, unidentified in
610 this work, overlap with the fluorescence of lignin. Further investigation are needs to
611 elucidate whose molecules are concerned. The main output is that there are higher
612 fluorescence signals of the hydroxycinnamate and both ‘lignin‘ and proteins at the FG
613 stage for the five cell types of the stems, without exception. The fluorescence intensities
614 decrease at the M stage.

After a 90° tilt of the flax stem, ~~generally,~~ the fluorescence intensity was higher in all five cell types. This molecular investigation shows that full histological flax stem organization is involved in the gravitropic response following tilting. Our data support the fact that the gravitropic response is also dependent on the metabolic activity of the plant, and the variations in proteins, hydroxycinnamates and lignin are influenced by the developmental stage when tilt occurs.

For cambium as well as the secondary xylem, the active cells are strongly affected by tilting, as demonstrated by a strong increase in the fluorescence intensity reflecting an increase of the metabolic activity. No cambial activity in the sense of cell divisions was measured in this work. So, in the sense of metabolic activity, if the gravitropic reaction occurs at plant maturity, cambial overfluorescence intensity in tilted plants is still present but is moderate compared to reactions occurring at vegetative or maturity stages.

The bast fibres were proven to also react after the stem tilt but moderately at the mature plant stage. No evidence of stem polarity generated after tilt was demonstrated by synchrotron DUV fluorescence imaging of the bast fibres, regardless of the developmental stage examined.

Acknowledgements

The authors are grateful to Marc Lahaye and Kevin Vidot for fruitful discussions. The authors acknowledge the financial support from SOLEIL for VV, CD and FC regarding Proposal 20171187. The authors also thank the French national research Network GDR 3710 INRAE/CNRS SYMBIOSE – Synthons et matériaux biosourcés for its support and the ANS μReshape' funding support received from the TRANSFORM department of INRAE. This research was also funded by the INTERREG VA FCE Program, FLOWER project, Grant Number 23.

References

Akin, D.E., 2013. Linen most useful: perspectives on structure, chemistry, and enzymes for retting flax. ISRN biotechnology 2013, 186534.

Allouche, F., Hanafi, M., Jamme, F., Robert, P., Guillon, F., Devaux, M.F., 2012. Coupling hyperspectral image data having different spatial resolutions by extending multivariate inter-battery Tucker analysis. Chemometrics and Intelligent Laboratory Systems 113, 43-51.

Arnould, O., Siniscalco, D., Bourmaud, A., Le Duigou, A., Baley, C., 2017. Better insight into the nano-mechanical properties of flax fibre cell walls. Industrial Crops and Products 97, 224-228.

Baldacci-Cresp, F., Spriet, C., Twyffels, L., Blervacq, A.-S., Neutelings, G., Baucher, M., Hawkins, S., 2020. A rapid and quantitative safranin-based fluorescent microscopy method to evaluate cell wall lignification. 102, 1074-1089.

Beaugrand, J., Nottez, M., Konnerth, J., Bourmaud, A., 2014. Multi-scale analysis of the structure and mechanical performance of woody hemp core and the dependence on the sampling location. Industrial Crops and Products 60, 193-204.

Bourmaud, A., Beaugrand, J., Shah, D.U., Placet, V., Baley, C., 2018. Towards the design of high-performance plant fibre composites. Progress in Materials Science 97, 347-408.

Bourmaud, A., Gibaud, M., Baley, C., 2016. Impact of the seeding rate on flax stem stability and the mechanical properties of elementary fibres. Industrial Crops and Products 80, 17-25.

Bourmaud, A., Mérotte, J., Siniscalco, D., Le Gall, M., Gager, V., Le Duigou, A., Pierre, F., Behlouli, K., Arnould, O., Beaugrand, J., Baley, C., 2019. Main criteria of sustainable natural fibre for efficient unidirectional biocomposites. Composites Part A: Applied Science and Manufacturing 124, 105504.

Buchanan, B.B., Gruissem, W., Jones, R.L., 2000. Biochemistry & molecular biology of plants. American Society of Plant Physiologists, Rockville, Md.

Chabi, M., Goulas, E., Leclercq, C.C., de Waele, I., Rihouey, C., Cenci, U., Day, A., Blervacq, A.S., Neutelings, G., Duponchel, L., Lerouge, P., Hausman, J.F., Renaut, J., Hawkins, S., 2017. A Cell Wall Proteome and Targeted Cell Wall Analyses Provide Novel Information on Hemicellulose Metabolism in Flax. Molecular & Cellular Proteomics 16, 1634-1651.

Corbin, C., Decourtil, C., Marosevic, D., Bailly, M., Lopez, T., Renouard, S., Doussot, J., Dutilleul, C., Auguin, D., Giglioli-Guivarc'h, N., Laine, E., Lamblin, F., Hano, C., 2013. Role of protein farnesylation events in the ABA-mediated regulation of the Pinoresinol-Lariciresinol Reductase 1 (LuPLR1) gene expression and lignan biosynthesis in flax (Linum usitatissimum L.). Plant Physiology and Biochemistry 72, 96-111.

Corbin, C., Drouet, S., Markulin, L., Auguin, D., Laine, E., Davin, L.B., Cort, J.R., Lewis, N.G., Hano, C., 2018. A genome-wide analysis of the flax (Linum usitatissimum L.) dirigent protein family: from gene identification and evolution to differential regulation. Plant Molecular Biology 97, 73-101.

Day, A., 2004. La lignification des fibres périphloémiennes du lin (Linum usitatissimum L.) : approches cytochimique, chimique et moléculaire, pp. 1 vol. (XI-253 f.).

Day, A., Fenart, S., Neutelings, G., Hawkins, S., Rolando, C., Tokarski, C., 2013. Identification of cell wall proteins in the flax (Linum usitatissimum) stem. Proteomics 13, 812-825.

Devaux, M.-F., Jamme, F., André, W., Bouchet, B., Alvarado, C., Durand, S., Robert, P., Saulnier, L., Bonnin, E., Guillon, F., 2018a. Synchrotron Time-Lapse Imaging of Lignocellulosic Biomass Hydrolysis: Tracking Enzyme Localization by Protein Autofluorescence and Biochemical Modification of Cell Walls by Microfluidic Infrared Microspectroscopy. Frontiers in Plant Science 9.

Devaux, M.F., Jamme, F., Andre, W., Bouchet, B., Alvarado, C., Durand, S., Robert, P., Saulnier, L., Bonnin, E., Guillon, F., 2018b. Synchrotron Time-Lapse Imaging of Lignocellulosic Biomass Hydrolysis: Tracking Enzyme Localization by Protein Autofluorescence and Biochemical

690 Modification of Cell Walls by Microfluidic Infrared Microspectroscopy. Frontiers in Plant Science
691 9, 16.
692 Dymińska, L., Gągor, A., Hanuza, J., Kulma, A., Preisner, M., Żuk, M., Szatkowski, M., Szopa, J.,
693 2014. Spectroscopic characterization of genetically modified flax fibers. Journal of Molecular
694 Structure 1074, 321-329.
695 Edelstein, A., Amodaj, N., Hoover, K., Vale, R., Stuurman, N., 2010. Computer control of
696 microscopes using μManager. Current protocols in molecular biology Chapter 14, Unit14.20.
697 Frédéric, J., Slavka, K., Sandrine, V., Fatma, A., Stéphane, P., Valérie, R., Matthieu, R., 2013. Deep
698 UV autofluorescence microscopy for cell biology and tissue histology. Biology of the Cell 105, 277-
699 288.
700 Ghislain, B., Clair, B., 2017. Diversity in the organisation and lignification of tension wood fibre
701 walls - A review. Iawa Journal 38, 245-265.
702 Gierlinger, N., Goswami, L., Schmidt, M., Burgert, I., Coutand, C., Rogge, T., Schwanninger, M.,
703 2008. In situ FT-IR microscopic study on enzymatic treatment of poplar wood cross-sections.
704 Biomacromolecules 9, 2194-2201.
705 Giuliani, A., Jamme, F., Rouam, V., Wien, F., Giorgetta, J.L., Lagarde, B., Chubar, O., Bac, S., Yao,
706 I., Rey, S., Herbeaux, C., Marlats, J.L., Zerbib, D., Polack, F., Refregiers, M., 2009. DISCO: a low-
707 energy multipurpose beamline at synchrotron SOLEIL. Journal of Synchrotron Radiation 16, 835-
708 841.
709 Gorshkova, T., Mokshina, N., Chernova, T., Ibragimova, N., Salnikov, V., Mikshina, P., Tryfona,
710 T., Banasiak, A., Immerzeel, P., Dupree, P., Mellerowicz, E.J., 2015. Aspen Tension Wood Fibers
711 Contain β-(1→4)-Galactans and Acidic Arabinogalactans Retained by Cellulose Microfibrils in
712 Gelatinous Walls. Plant Physiol 169, 2048.
713 Gorshkova, T.A., Chemikosova, S.B., Sal'nikov, V.V., Pavlencheva, N.V., Gur'janov, O.P., Stolle-
714 Smits, T., van Dam, J.E.G., 2004. Occurrence of cell-specific galactan is coinciding with bast fiber
715 developmental transition in flax. Industrial Crops & Products 19, 217-224.
716 Gorshkova, T.A., Salnikov, V.V., Chemikosova, S.B., Ageeva, M.V., Pavlencheva, N.V., Dam,
717 J.E.G., 2003. The snap point: a transition point in Linum usitatissimum bast fiber development. Ind
718 Crops Prod. 18.
719 Gorshkova, T.A., Salnikov, V.V., Pogodina, N.M., Chemikosova, S.B., Yablokova, E.V., Ulanov,
720 A.V., Ageeva, M.V., Van Dam, J.E.G., Lozovaya, V.V., 2000. Composition and distribution of cell
721 wall phenolic compounds in flax (Linum usitatissimum L.) stem tissues. Ann. Bot. 85, 477-486.
722 Gorshkova, T.A., Wyatt, S.E., Salnikov, V.V., Gibeaut, D.M., Ibragimov, M.R., Lozovaya, V.V.,
723 Carpita, N.C., 1996. Cell-Wall Polysaccharides of Developing Flax Plants. Plant Physiol 110, 721-
724 729.
725 Goubet, F., Morvan, C., 1993. Evidence for several galactan synthases in flax (*Linum-Usitassimum*
726 *L*) suspension-cultured cells Plant and Cell Physiology 34, 1297-1303.
727 Goudenhooft, C., Bourmaud, A., Baley, C., 2017. Varietal selection of flax over time: Evolution of
728 plant architecture related to influence on the mechanical properties of fibers. Industrial Crops and
729 Products 97, 56-64.
730 Goudenhooft, C., Bourmaud, A., Baley, C., 2019a. Flax (Linum usitatissimum L.) Fibers for
731 Composite Reinforcement: Exploring the Link Between Plant Growth, Cell Walls Development,
732 and Fiber Properties. Frontiers in Plant Science 10.
733 Goudenhooft, C., Bourmaud, A., Baley, C., 2019b. Study of plant gravitropic response: Exploring
734 the influence of lodging and recovery on the mechanical performances of flax fibers. Industrial
735 Crops and Products 128, 235-238.
736 Goudenhooft, C., Siniscalco, D., Arnould, O., Bourmaud, A., Sire, O., Gorshkova, T., Baley, C.,
737 2018. Investigation of the Mechanical Properties of Flax Cell Walls during Plant Development: The
738 Relation between Performance and Cell Wall Structure. Fibers 6, 9.
739 Heer, 1873. Prehistoric Culture of Flax. Nature 7, 453-453.

Heller, K., Sheng, Q.C., Guan, F., Alexopoulou, E., Hua, L.S., Wu, G.W., Jankauskienė, Z., Fu, W.Y., 2015. A comparative study between Europe and China in crop management of two types of flax: linseed and fibre flax. Industrial Crops and Products 68, 24-31.
Himmelsbach, D.S., Khalili, S., Akin, D.E., 1998. FT-IR microspectroscopic imaging of flax (Linum usitatissimum L.) stems. Cellular and molecular biology (Noisy-le-Grand, France) 44, 99-108.
Ibragimova, N.N., Ageeva, M.V., Gorshkova, T.A., 2017. Development of gravitropic response: unusual behavior of flax phloem G-fibers. Protoplasma 254, 749-762.
Jamme, F., Bourquin, D., Tawil, G., Vikso-Nielsen, A., Buleon, A., Refregiers, M., 2014. 3D Imaging of Enzymes Working in Situ. Analytical Chemistry 86, 5265-5270.
Jamme, F., Kascakova, S., Villette, S., Allouche, F., Pallu, S., Rouam, V., Réfrégiers, M., 2013. Deep UV autofluorescence microscopy for cell biology and tissue histology. Biol Cell 105.
Le Roy, J., Blervacq, A.S., Creach, A., Huss, B., Hawkins, S., Neutelings, G., 2017. Spatial regulation of monolignol biosynthesis and laccase genes control developmental and stress-related lignin in flax. Bmc Plant Biology 17, 20.
Liao, Y., Koelewijn, S.-F., Van den Bossche, G., Van Aelst, J., Van den Bosch, S., Renders, T., Navare, K., Nicolaï, T., Van Aelst, K., Maesen, M., Matsushima, H., Thevelein, J.M., Van Acker, K., Lagrain, B., Verboekend, D., Sels, B.F., 2020. A sustainable wood biorefinery for low–carbon footprint chemicals production. 367, 1385-1390.
Lion, C., Simon, C., Huss, B., Blervacq, A.S., Tirot, L., Toybou, D., Spriet, C., Slomianny, C., Guerardel, Y., Hawkins, S., Biot, C., 2017. BLISS: A Bioorthogonal Dual-Labeling Strategy to Unravel Lignification Dynamics in Plants. Cell chemical biology 24, 326-338.
Maréchal, Y., Chanzy, H., 2000. The hydrogen bond network in I _β cellulose as observed by infrared spectrometry. 523, 183.
Mikshina, P.V., Gurjanov, O.P., Mukhitova, F.K., Petrova, A.A., Shashkov, A.S., Gorshkova, T.A., 2012. Structural details of pectic galactan from the secondary cell walls of flax (Linum usitatissimum L.) phloem fibres. Carbohydrate Polymers 87, 853-861.
Mnich, E., Bjarnholt, N., Eudes, A., Harholt, J., Holland, C., Jørgensen, B., Larsen, F.H., Liu, M., Manat, R., Meyer, A.S., Mikkelsen, J.D., Motawia, M.S., Muschiol, J., Møller, B.L., Møller, S.R., Perzon, A., Petersen, B.L., Ravn, J.L., Ulvskov, P., 2020. Phenolic cross-links: building and de-constructing the plant cell wall. Natural Product Reports.
Mohanty, A.K., Vivekanandhan, S., Pin, J.-M., Misra, M., 2018. Composites from renewable and sustainable resources: Challenges and innovations. Science 362, 536-542.
Monties, B., 1989. Molecular structure and biochemical properties of lignins in relation to possible self-organization of lignin networks, Annales des sciences forestières. EDP Sciences, pp. 848s-855s.
Nuez, L., Beaugrand, J., Shah, D.U., Mayer-Laigle, C., Bourmaud, A., D'Arras, P., Baley, C., 2020. The potential of flax shives as reinforcements for injection moulded polypropylene composites. Industrial Crops and Products 148, 112324.
Petrova, A., Kozlova, L., Gorshkov, O., Nazipova, A., Ageeva, M., Gorshkova, T., 2021. Cell Wall Layer Induced in Xylem Fibers of Flax Upon Gravistimulation Is Similar to Constitutively Formed Cell Walls of Bast Fibers. 12.
Petrova, A.A., Kozlova, L.V., Gaifullina, I.Z., Ananchenko, B.A., Martinson, E.A., Mikshina, P.V., Gorshkova, T.A., 2019. AFM analysis reveals polymorphism of purified flax rhamnogalacturonans I of distinct functional types. Carbohydrate Polymers 216, 238-246.
Ray F. Evert, S.E.E., 2006. Esau's Plant Anatomy: Meristems, Cells, and Tissues of the Plant Body: Their Structure, Function, and Development, 3rd Edition. 624.
Réquilé, S., Goudenhooft, C., Bourmaud, A., Le Duigou, A., Baley, C., 2018. Exploring the link between flexural behaviour of hemp and flax stems and fibre stiffness. Industrial Crops and Products 113, 179-186.

Roach, M.J., Mokshina, N.Y., Badhan, A., Snegireva, A.V., Hobson, N., Deyholos, M.K., Gorshkova, T.A., 2011. Development of cellulosic secondary walls in flax fibers requires beta-galactosidase. Plant Physiol 156, 1351-1363.
Scalbert, A., Monties, B., Lallemand, J.-Y., Guittet, E., Rolando, C.J.P., 1985. Ether linkage between phenolic acids and lignin fractions from wheat straw. 24, 1359-1362.
Stewart, D., McDougall, G.J., Baty, A., 1995. Fourier-Transform Infrared Microspectroscopy of Anatomically Different Cells of Flax (Linum usitatissimum) Stems during Development. Journal of Agricultural and Food Chemistry 43, 1853-1858.
Tomazevic, D., Likar, B., Pernus, F., 2002. Comparative evaluation of retrospective shading correction methods. Journal of microscopy 208, 212-223.
Viala, R., Placet, V., Cogan, S., 2018. Identification of the anisotropic elastic and damping properties of complex shape composite parts using an inverse method based on finite element model updating and 3D velocity fields measurements (FEMU-3DVF): Application to bio-based composite violin soundboards. Composites Part a-Applied Science and Manufacturing 106, 91-103.

Figures caption

Figure 1. Scheme of the different steps of the experiment. The top part: a) Schematic representation of the flax stems at different maturity stages. The pots were never inclined and so acted as control (*_C*) conditions, whereas other pots were tilted for 4 days. Tilting (*_90*) was performed at three major stages of plant development (*VS*, *FG* and *M*), and tilted samples were collected 4 days after tilting, as depicted in the lower part b). About 10 cm stem portions taken approximately 2 cm above cotyledons were sampled from whole stems and are illustrated by blue rectangles in b). Overall, 6 flax stem conditions were explored (*VS_C, VS_90, FG_C, FG_90, M_C and M_90*).

Figure 2. Individual channel fluorescence and composite view of the VS_C flax stem cross section. a) Fluorescence intensity of the channel of proteins, b) channel of hydroxycinnamate in c) channel of lignin, d) the composite view with the merged a-c channels, in e) a guide to interpret colours and in f) a phloroglucinol staining of the quarter of the stem section to present the 5 cellular components of this study. The field of view is 2.7 x 2.5 mm² for images a to d. In f, the inner stem part to the epidermis is (ep),

820 the bast fibre (bf), the cambium (ca), the xylem - secondary (xs) and the xylem - primary
821 (xp).

822 **Figure 3.** Composite fluorescence images of the control plants *_C* or tilted plants *_90*,
823 magnification 10x. Stem cross section from a control plant (a) and from a tilted plant (d)
824 during the vegetative stage VS. Stem cross section from control (b) and tilted (e) plants
825 during fast growth *FG*. Stem cross section of mature *M* plants and control (c) and tilted (f)
826 plants. In b, a caudal pod is visible on the left side of the stem.

827 **Figure 4.** Fluorescence measurement in the cell types. A is the full stem section with the
828 4 sampling areas (labelled 1, 2, 3 and 4). The different cell types selected for
829 fluorescence intensity quantification are indicated. B focuses on area 1 to illustrate the
830 manual selection of pixels in the different cell types; the red lines go from the outer part to
831 the inner stem part to the epidermis (ep), the bast fibre (bf), the cambium (ca), the xylem -
832 secondary (xs) and the xylem - primary (xp). A zoom is provided for each vignette.

833 **Figure 5.** Average values of the fluorescence intensity (in arbitrary units) obtained from
834 the ANOVA development stages × conditions. The drop caps indicate whether the values
835 are significantly different from each other or not.

836 **Figure 6.** Cellular type average fluorescence intensity according to development and tilting
837 conditions. The drop caps indicate whether the values are significantly different from each
838 other or not.
839 **Figure 7.** FTIR spectrum of bast fibres.

840 In a), the blue dots indicate the location of the bast fibre local spectra collected around
841 the flax stem samples. In b), the absorption bands for the main components in bast fibre
842 are indicated.

Figure 8. Effect of the development stage. The bast fibre second-derivative micro-FTIR spectral signals of control plants are superimposed. Red arrows indicate the bands of interest for the study.

Figure 9. Effect of a 90° tilt on the second-derivative micro-FTIR spectra of the flax bast fibre. Red arrows indicate the bands of interest for the study.

Figure 10. Investigation of the putative polarity in the stem by exploring the fluorescence of control versus tilted stems in bast fibres. Fig 10a) shows the arbitrary positioning of the fluorescence measurements around the stem section. Fig 10b) shows the location of the pixel fluorescence measurement in the bast fibre for M_C (square) and M_90 (lozenge). Fig 10c) shows the fluorescence intensity measured and expressed linearly for the tilted/untreated plants.

Table caption

Table 1. Building colour images from the three emission filters. The same maximum intensity values were set for all images.

Figure 1. Scheme of the different steps of the experiment. The top part: a) Schematic representation of the flax stems at different maturity stages. The pots were never inclined and so acted as control (*_C*) conditions, whereas other pots were tilted for 4 days. Tilting (*_90*) was performed at three major stages of plant development (*VS*, *FG* and *M*), and tilted samples were collected 4 days after tilting, as depicted in the lower part b). About 10 cm stem portions taken approximately 2 cm above cotyledons were sampled from whole stems and are illustrated by blue rectangles in b). Overall, 6 flax stem conditions were explored (*VS_C, VS_90, FG_C, FG_90, M_C and M_90*).

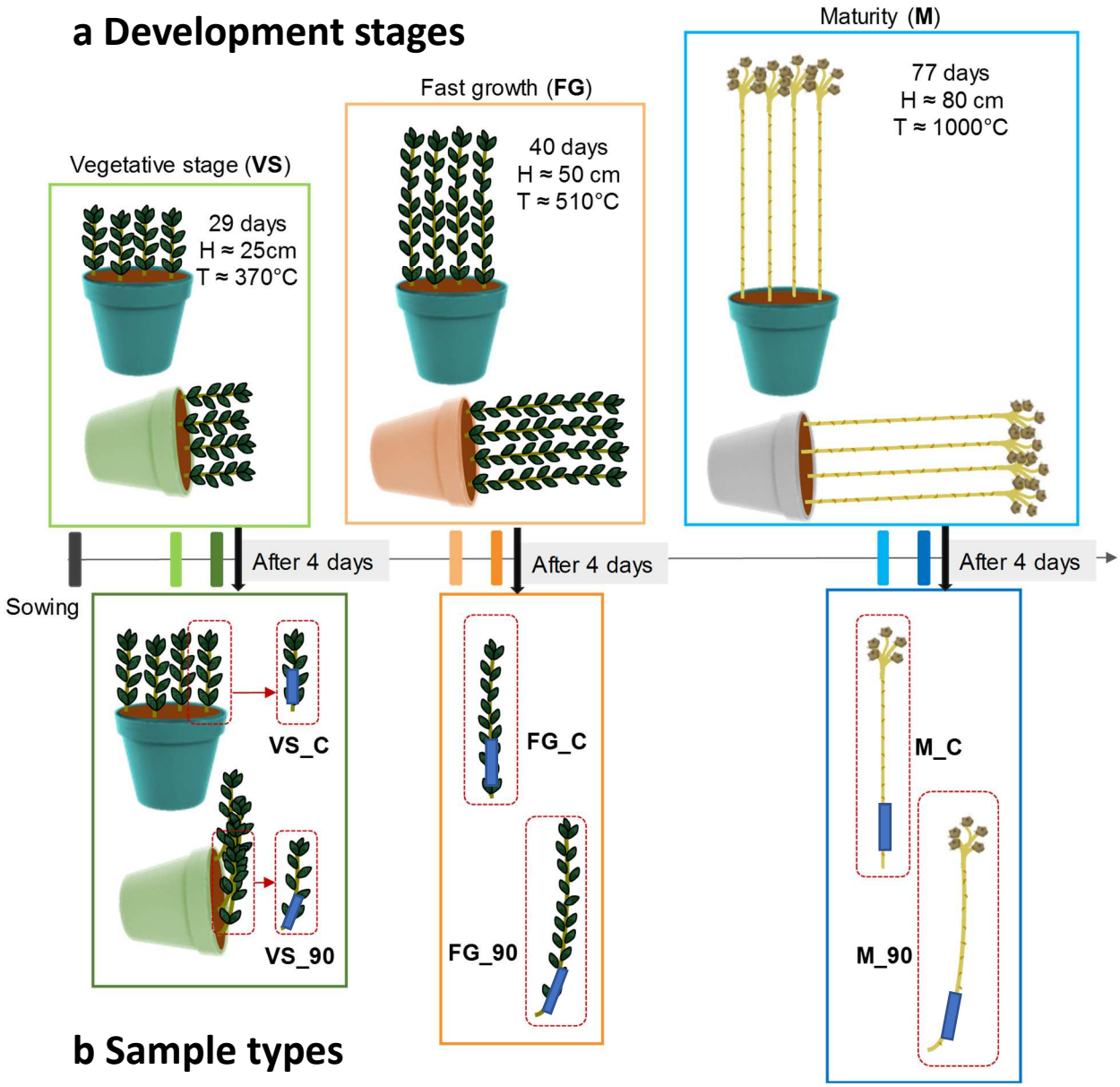

Figure 2. Individual channel fluorescence and composite view of the VS_C flax stem cross section. a) Fluorescence intensity of the channel of proteins, b) channel of hydroxycinnamate in c) channel of lignin, d) the composite view with the merged a-c channels, in e) a guide to interpret colours and in f) a phloroglucinol staining of the quarter of the stem section to present the 5 cellular components of this study. The field of view is 2.7 x 2.5 mm² for images a to d. In f, the inner stem part to the epidermis is (ep), the bast fibre (bf), the cambium (ca), the xylem - secondary (xs) and the xylem - primary (xp).

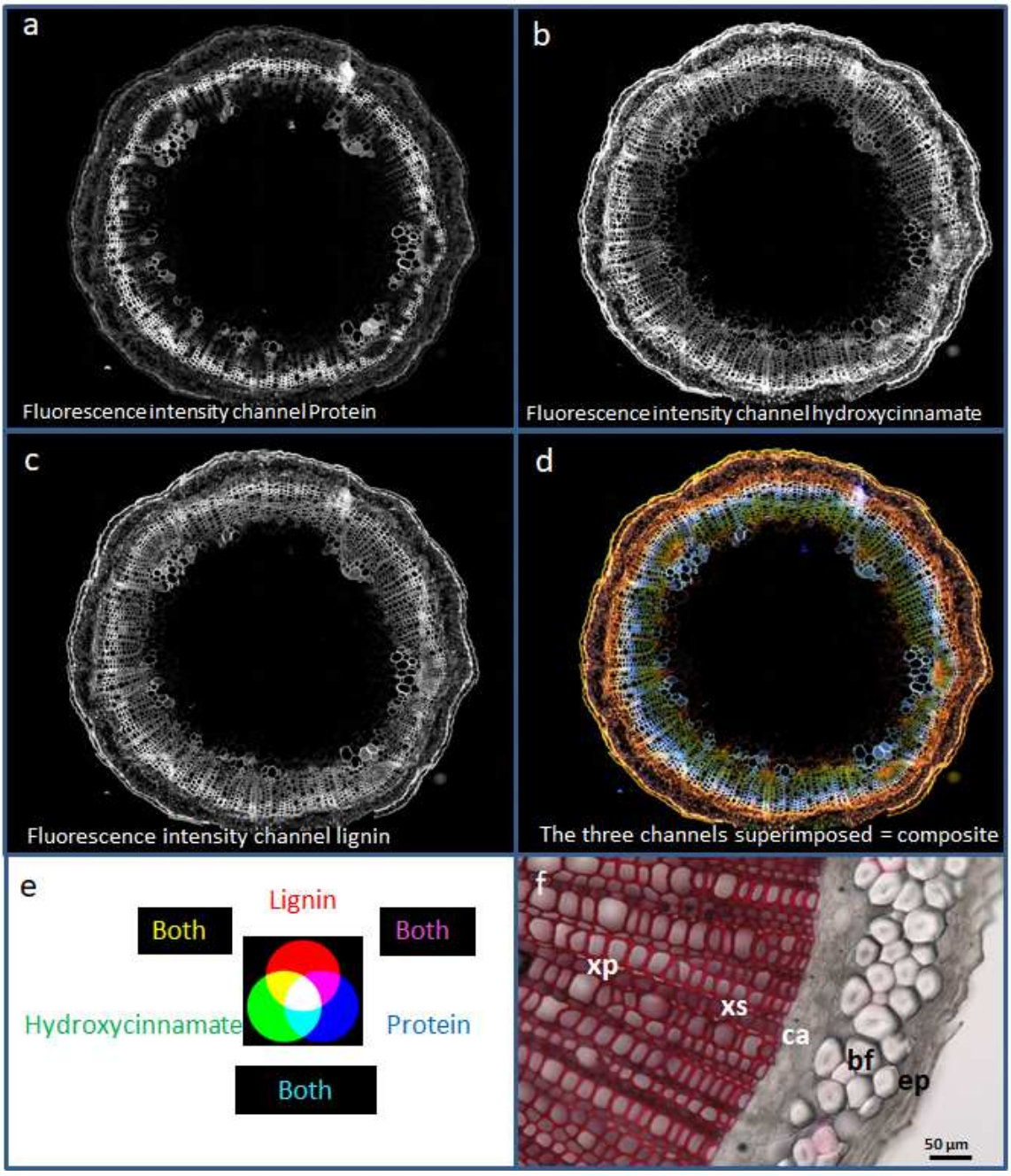

Figure 3. Composite fluorescence images of the control plants *_C* or tilted plants *_90*, magnification 10x. Stem cross section from a control plant (a) and from a tilted plant (d) during the vegetative stage VS. Stem cross section from control (b) and tilted (e) plants during fast growth *FG*. Stem cross section of mature *M* plants and control (c) and tilted (f) plants. In b, a caudal pod is visible on the left side of the stem.

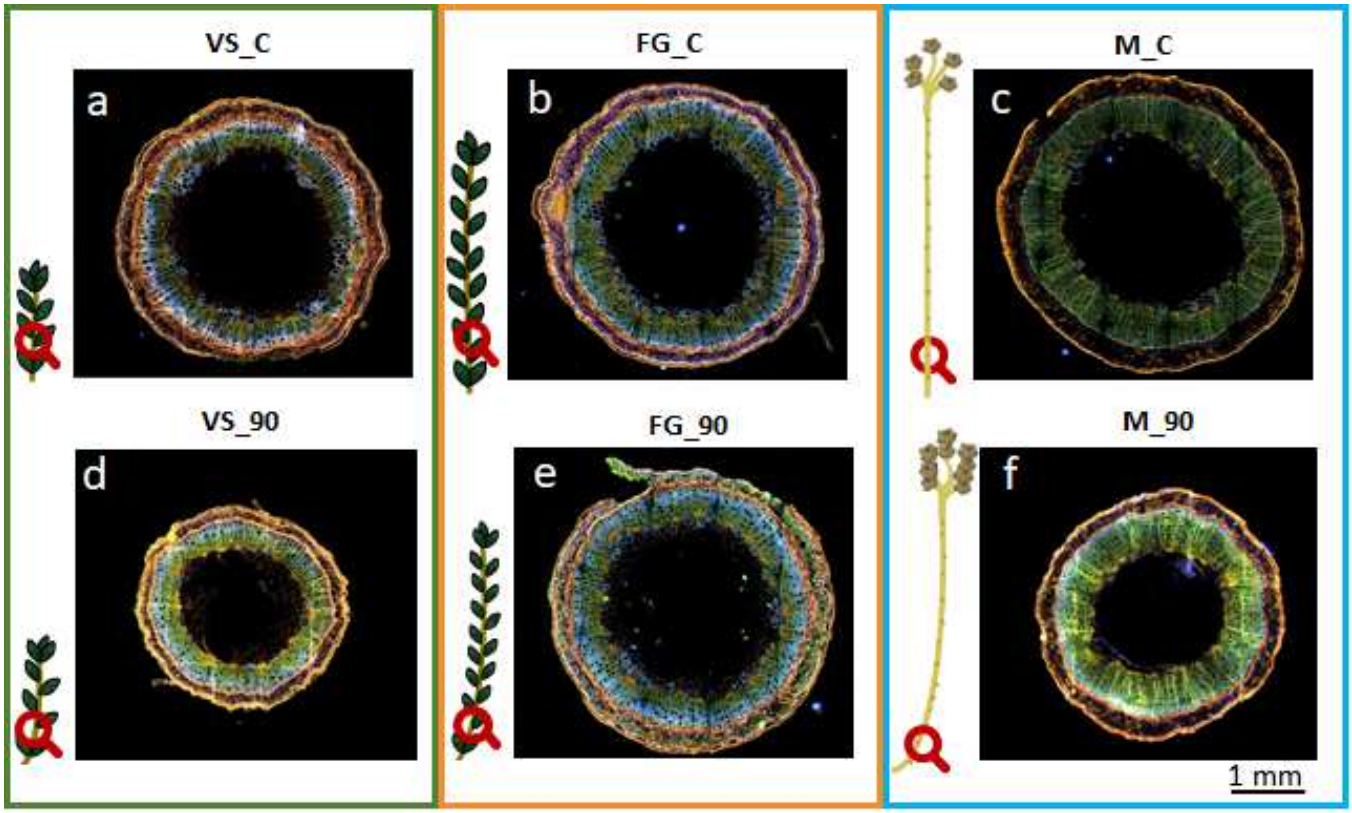

Figure 4. Fluorescence measurement in the cell types. A is the full stem section with the 4 sampling areas (labelled 1, 2, 3 and 4). The different cell types selected for fluorescence intensity quantification are indicated. B focuses on area 1 to illustrate the manual selection of pixels in the different cell types; the red lines go from the outer part to the inner stem part to the epidermis (ep), the bast fibre (bf), the cambium (ca), the xylem - secondary (xs) and the xylem - primary (xp). A zoom is provided for each vignette.

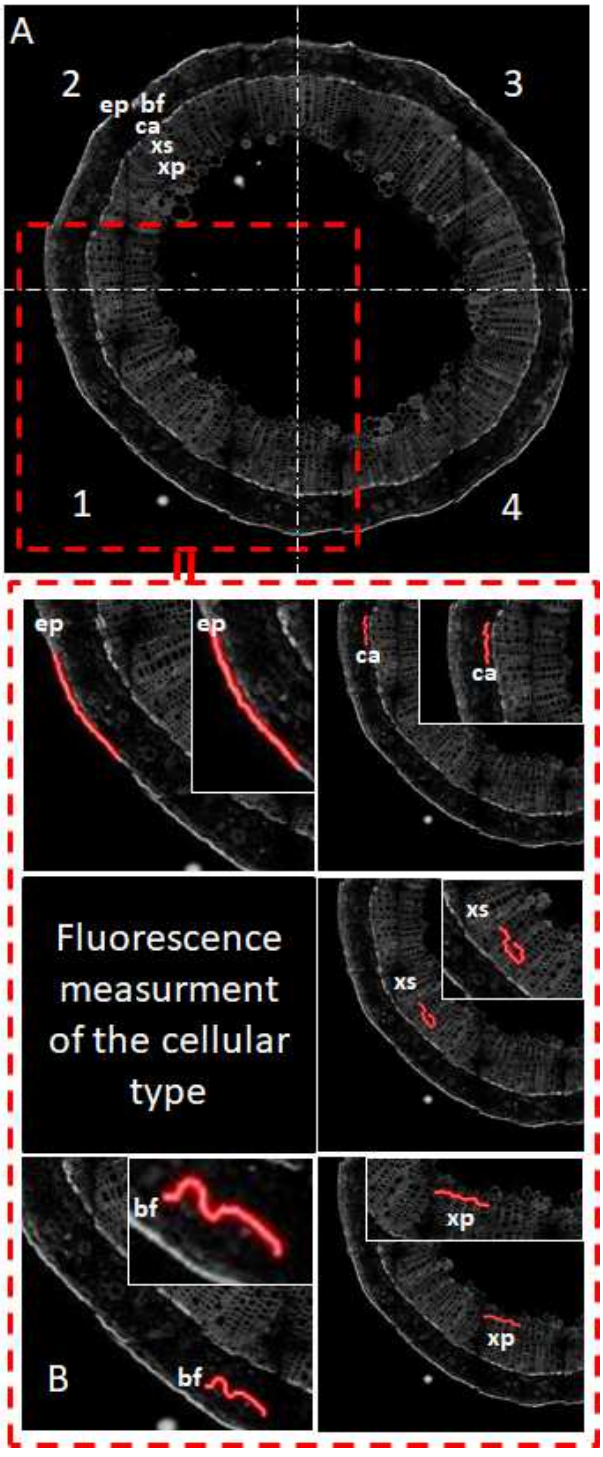

Figure 5. Average values of the fluorescence intensity (in arbitrary units) obtained from the ANOVA development stages × conditions. The drop caps indicate whether the values are significantly different from each other or not.

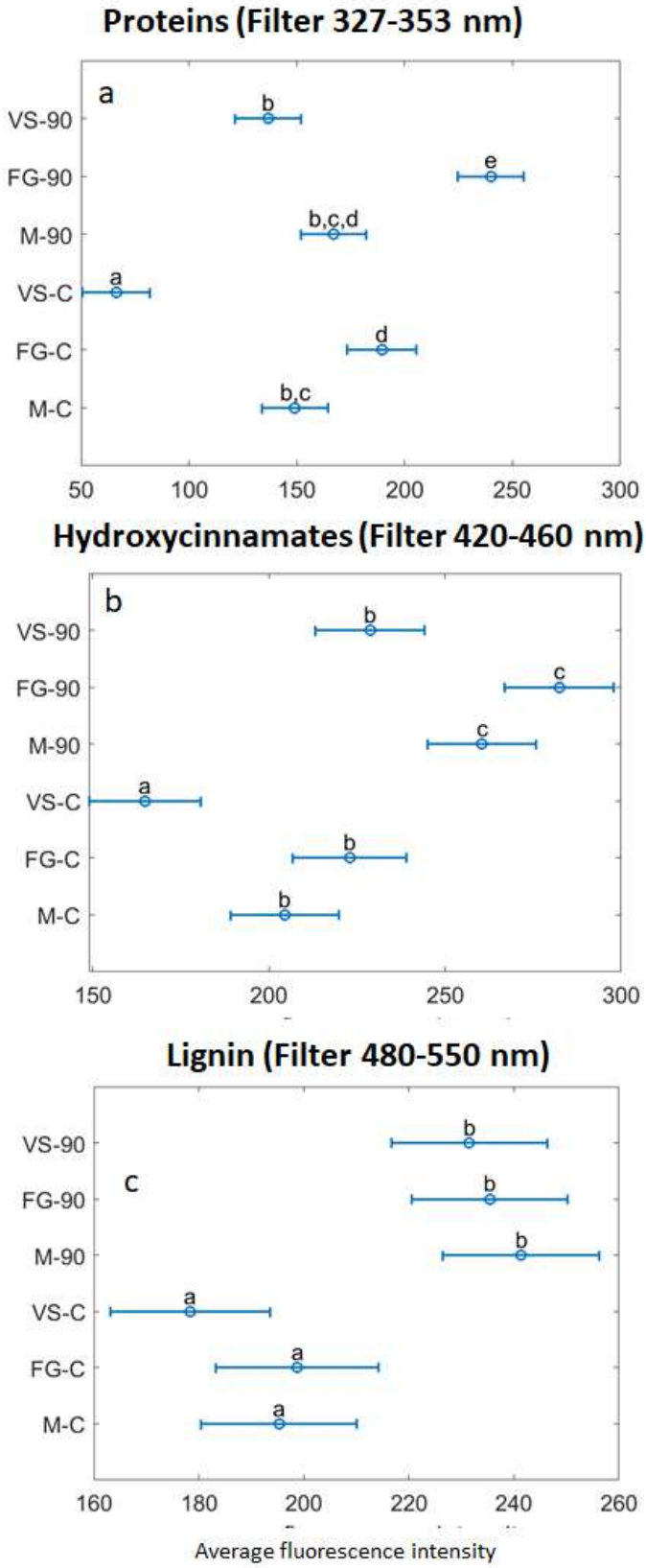

Figure 6. Cellular type average fluorescence intensity according to development and tilting conditions. The drop caps indicate whether the values are significantly different from each other or not.

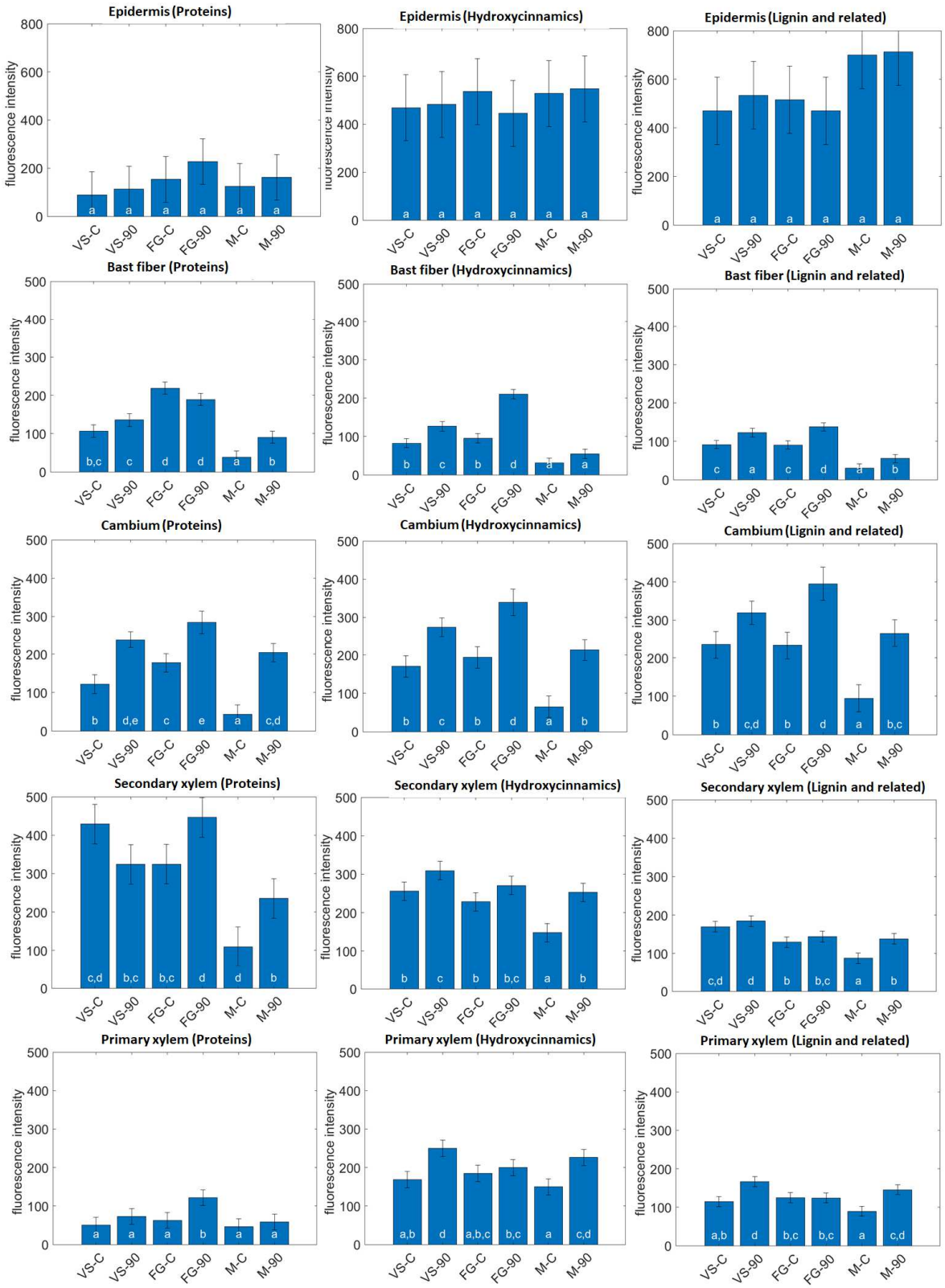

Figure 7. FTIR spectrum of bast fibres.

In a), the blue dots indicate the location of the bast fibre local spectra collected around the flax stem samples. In b), the absorption bands for the main components in bast fibre are indicated.

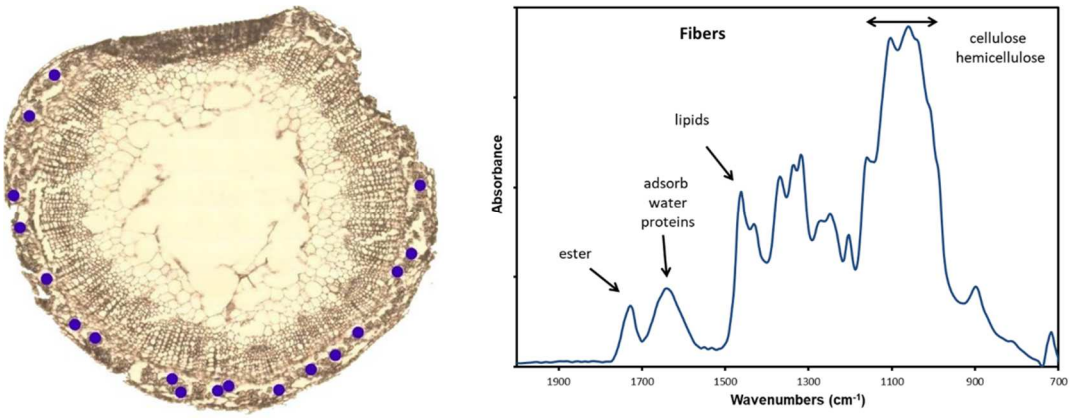

Figure 8. Effect of the development stage. The bast fibre second-derivative micro-FTIR spectral signals of control plants are superimposed. Red arrows indicate the bands of interest for the study.

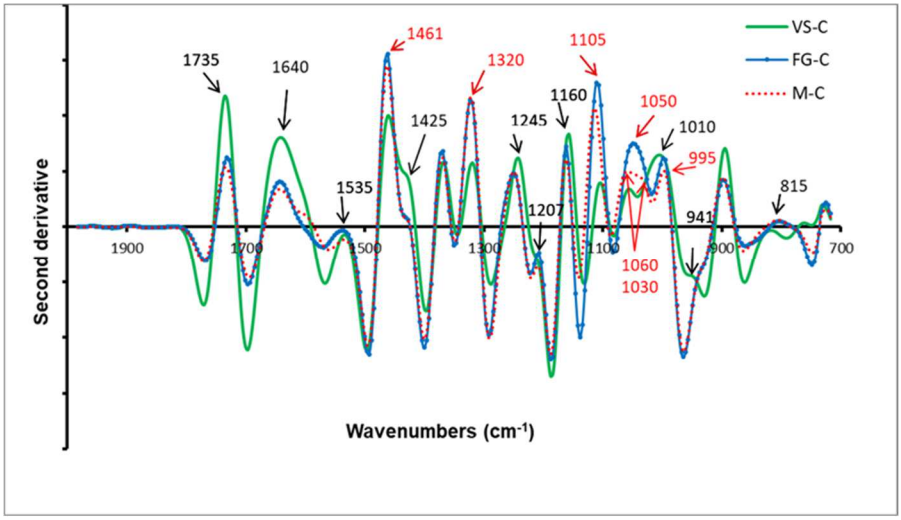

Figure 9. Effect of a 90° tilt on the second-derivative micro-FTIR spectra of the flax bast fibre. Red arrows indicate the bands of interest for the study.

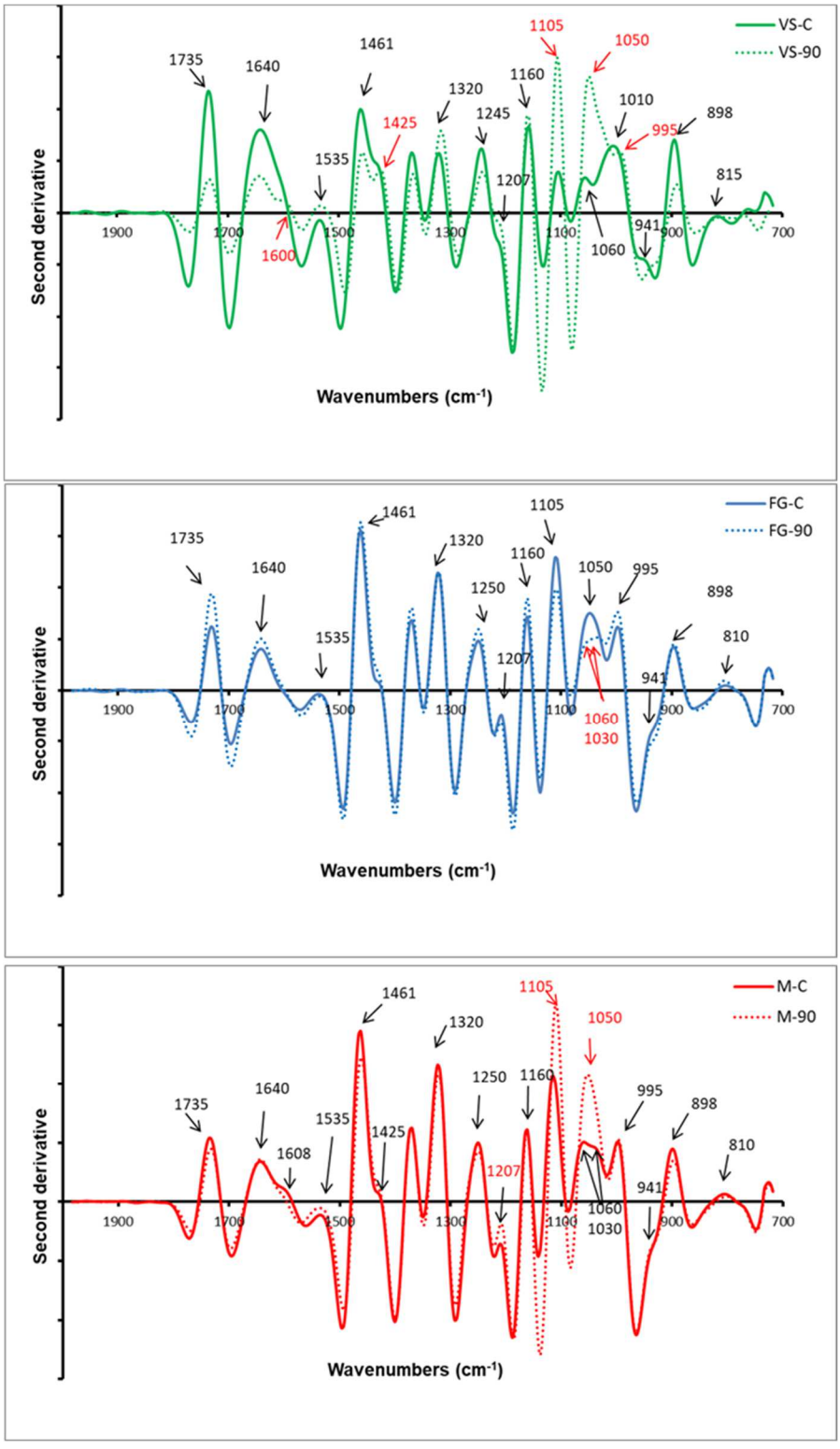

Figure 10. Investigation of the putative polarity in the stem by exploring the fluorescence of control versus tilted stems in bast fibres. Fig 10a) shows the arbitrary positioning of the fluorescence measurements around the stem section. Fig 10b) shows the location of the pixel fluorescence measurement in the bast fibre for M_C (square) and M_90 (lozenge). Fig 10c) shows the fluorescence intensity measured and expressed linearly for the tilted/untreated plants.

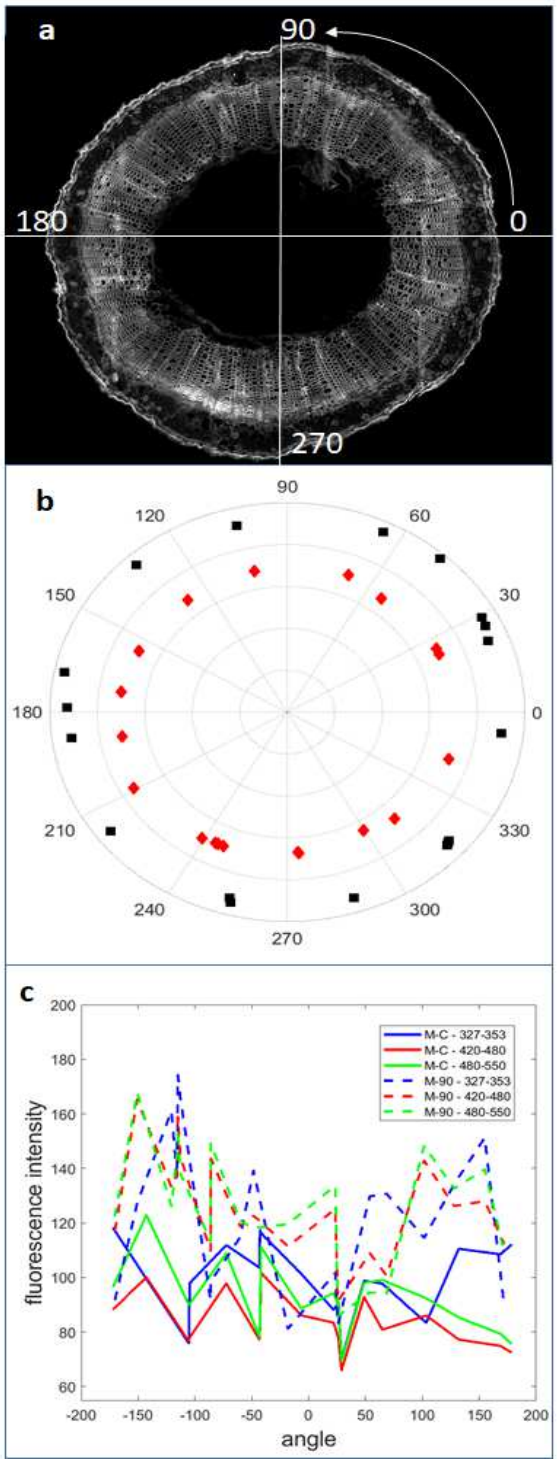

Table 1. Building colour images from the three emission filters. The same maximum intensity values were set for all images.

Channel of the colour image	Filter / bandpass	Maximum intensity	Expected compound	Expected colour
Blue	327-353 nm	500	Protein	blue
Green	420-460 nm	400	Hydroxycinnamates	Green to yellow
Red	480-550 nm	300	Lignin	Red to yellow

Development



of flax stems


& gravitropism

λ_{Ex} = 274.984 nm

Proteins (Blue)	λ_{Em} 327–353 nm
Hydroxycinnamats -Green)	λ_{Em} 420–460 nm
Lignin and unidentified (Red)	λ_{Em} 480–550 nm

Qualitative and quantitative

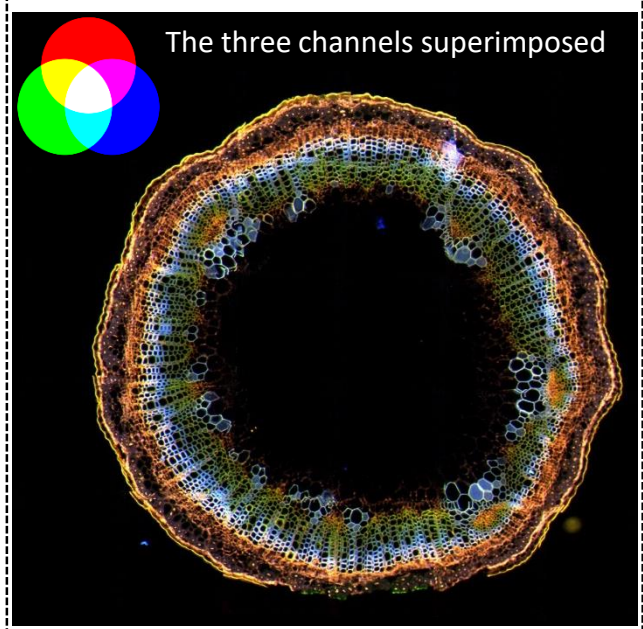

biochemical mapping